J|A|C|S ARTICLES

Published on Web 10/07/2010

Solution-Phase Synthesis of Heteroatom-Substituted Carbon Scaffolds for Hydrogen Storage

Zhong Jin,[†] Zhengzong Sun,[†] Lin J. Simpson,[‡] Kevin J. O'Neill,[‡] Philip A. Parilla,[‡] Yan Li,[§] Nicholas P. Stadie,[||] Channing C. Ahn,*[,||] Carter Kittrell,*[,†] and James M. Tour*[,†]

Department of Chemistry, Department of Mechanical Engineering and Materials Science, and The Richard E. Smalley Institute for Nanoscale Science and Technology, Rice University, MS-222, 6100 Main Street, Houston, Texas 77005, United States, National Renewable Energy Laboratory, 1617 Cole Boulevard, Golden, Colorado 80401, United States, College of Chemistry and Molecular Engineering, Peking University, Beijing 100871, P. R. China, and W. M. Keck Laboratory, California Institute of Technology, 138-78, Pasadena, California 91125, United States

Received June 21, 2010; E-mail: cca@caltech.edu; kittrell@rice.edu; tour@rice.edu

Abstract: This paper reports a bottom-up solution-phase process for the preparation of pristine and heteroatom (boron, phosphorus, or nitrogen)-substituted carbon scaffolds that show good surface areas and enhanced hydrogen adsorption capacities and binding energies. The synthesis method involves heating chlorine-containing small organic molecules with metallic sodium at reflux in high-boiling solvents. For heteroatom incorporation, heteroatomic electrophiles are added to the reaction mixture. Under the reaction conditions, micrometer-sized graphitic sheets assembled by 3−5 nm-sized domains of graphene nanoflakes are formed, and when they are heteroatom-substituted, the heteroatoms are uniformly distributed. The substituted carbon scaffolds enriched with heteroatoms (boron ∼7.3%, phosphorus ∼8.1%, and nitrogen ∼28.1%) had surface areas as high as 900 m^2 g^{-1} and enhanced reversible hydrogen physisorption capacities relative to pristine carbon scaffolds or common carbonaceous materials. In addition, the binding energies of the substituted carbon scaffolds, as measured by adsorption isotherms, were 8.6, 8.3, and 5.6 kJ mol^{-1} for the boron-, phosphorus-, and nitrogen-enriched carbon scaffolds, respectively.

Introduction

Hydrogen is a promising energy carrier that may supplement or replace nonrenewable fuels such as oil, natural gas, and coal in future energy systems.[1,2] An especially valuable application is in hydrogen-powered vehicles. Hydrogen is a cleaner energy source than hydrocarbon fuels: a hydrogen-powered vehicle emits no pollutants into the local environment and releases a reduced amount of carbon dioxide into the atmosphere per mile driven in comparison with a hydrocarbon-fueled internal combustion engine. Since hydrogen can be readily produced from wind and solar power, it could become a carbon- and pollution-free source of energy for vehicle propulsion. However, the facile storage of hydrogen with high capacity in a compact tank remains a challenging problem.

Currently, there are several approaches to the storage of hydrogen.[3−5] High-pressure tanks are used on demonstration vehicles; however, they are bulky and have limited capacity, and conformal architectures that use on-board space more efficiently are not feasible because of the high pressures (5000−10000 psi or 350−700 atm), which dictate the use of high-strength composite tanks. Storage of cryogenic liquid hydrogen is costly, and its production is energy-intensive. Metal hydrides show promise for storage of hydrogen in the solid state; however, the exothermic reaction that takes place upon hydrogen evolution remains a problem, and metal hydrides can also have problems with gravimetric capacities or kinetics of delivery. Chemical hydrides generally require off-board regeneration, lowering the well-to-tank efficiency. Media that store hydrogen in molecular form could have many attractive features in some embodiments, such as minimal energy consumption for adsorption/desorption, facile kinetics, less demanding thermal management ranges, and unlimited cycling since no covalent chemical reaction is involved. High-surface-area adsorbents such as porous carbon materials, metal−organic frameworks, and porous polymers are being studied and evaluated for this purpose. Carbonaceous adsorbents such as activated carbon and sp^2 graphitic carbon systems, including carbon nanotubes,[6,7] have attracted much interest; however, the low binding energy of

[†] Rice University.
[‡] National Renewable Energy Laboratory.
[§] Peking University.
[||] California Institute of Technology.

(1) U.S. Department of Energy Office of Energy Efficiency and Renewable Energy. Fuel Cell Technologies Program: Hydrogen Storage. http://www1.eere.energy.gov/hydrogenandfuelcells/storage/ (accessed June 15, 2010).
(2) Satyapal, S.; Petrovic, J.; Read, C.; Thomas, G.; Ordaz, G. *Catal. Today* **2007**, *120*, 246.
(3) Felderhoff, M.; Weidenthaler, C.; von Helmolt, R.; Eberle, U. *Phys. Chem. Chem. Phys.* **2007**, *9*, 2643.
(4) Eberle, U.; Felderhoff, M.; Schuth, F. *Angew. Chem., Int. Ed.* **2009**, *48*, 6608.
(5) Morris, R. E.; Wheatley, P. S. *Angew. Chem., Int. Ed.* **2008**, *47*, 4966.
(6) Rao, C. N. R.; Satishkumar, B. C.; Govindaraj, A.; Nath, M. *ChemPhysChem* **2001**, *2*, 78.

 10.1021/ja105428d

Scheme 1. Bottom-Up Preparation of Heteroatom-Substituted Carbon Scaffolds by a Solution-Phase Process[a]

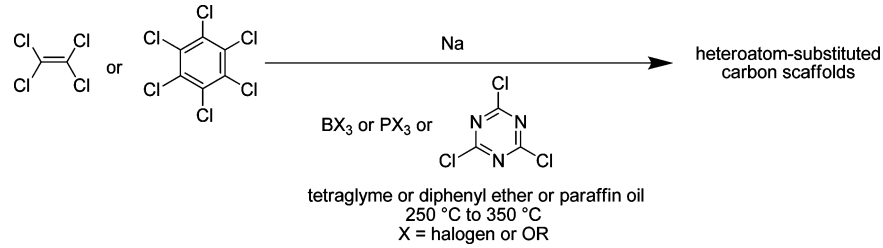

[a] The pristine carbon scaffolds were prepared in the same manner but without the boron-, phosphorus-, or nitrogen-containing precursor.

molecular hydrogen on the carbon surface requires cryogenic cooling, which increases the mass and volume of the container, thereby reducing the gravimetric and volumetric capacity for hydrogen.

In carbonaceous materials, the hydrogen physisorption surface excess capacity can typically reach 1 wt % H_2 per 500 m^2 g^{-1} specific surface area at 77 K at the asymptotic pressure of ~40 bar, according to Chahine's rule.[8] Additionally, the binding energy of hydrogen to the carbon surface is low (4−6 kJ mol^{-1}),[9,10] although well-defined microporosity may significantly increase the binding energy.[11] To further increase the binding energy, different routes have been explored, such as the development of new carbon materials with engineered nanospaces[7,12] as well as metal functionalization that may polarize the H_2 molecule.[13,14] Recent theoretical and experimental investigations have shown that it is possible to improve the hydrogen binding energy and hydrogen adsorption capacity of carbon materials by heteroatom substitution, such as boron[15−18] or nitrogen substitution,[19,20] depending on the type and concentration of heteroatom. To obtain both high surface area and high heteroatom concentration, the bottom-up synthesis of heteroatom-substituted carbon materials from carbon- and heteroatom-containing precursors in the solution phase can be an effective approach. For example, Mu et al.[21] have prepared carbon/nitrogen nanotubes and nanofibers by solvothermal methods. Here we report a facile bottom-up solution-phase approach for the direct synthesis of heteroatom-substituted carbon scaffolds containing boron, phosphorus, or nitrogen atoms at high and controllable concentrations. These heteroatom-substituted carbon scaffolds have improved reversible hydrogen uptake relative to typical porous carbon materials. Although the present work is still dependent on cryogenic use of hydrogen, the scalable synthetic protocol and the enhanced binding energies achieved illustrate the efficacy of the heteroatom substitution effect in synthetic carbon formulations.

Experimental Section

Bottom-Up Preparation of Synthetic Carbon Scaffolds. The pristine and heteroatom-substituted carbon scaffolds were prepared by refluxing chloro-substituted organic reagents containing sp^2 carbon and chosen heteroatom precursors together with sodium in high-boiling solvents, as shown in Scheme 1. Typically, 50 mL of tetraglyme, diphenyl ether (warmed above 26 °C), or paraffin oil was placed in a 100 mL nitrogen-purged and oven-dried three-neck round-bottom flask equipped with a magnetic stir bar, a nitrogen gas inlet, a stopper, and an air reflux condenser connected to an oil bubbler. Tetrachloroethylene (1.2 mL, 10 mmol) or hexachlorobenzene (0.94 g, 3.3 mmol) was added to the solvent as the carbon source. Next, 20 mmol of triisopropyl borate, triethyl phosphite, or cyanuric chloride and freshly cut sodium (2.6 g, 113 mequiv) were slowly added to the mixture under a nitrogen gas flow. In the preparation of pristine carbon scaffolds, no heteroatom reagent and less sodium (1.2 g, 60 mequiv) was used. For the heteroatom-substituted carbon scaffolds, triisopropyl borate, triethyl phosphite, and cyanuric chloride were used as the boron, phosphorus, and nitrogen sources, respectively. Alternatively, boron trichloride and phosphorus trichloride also could serve as boron and phosphorus sources, respectively; both are air-sensitive and should be handled in the glovebox. Two heteroatom precursors with different substitution elements could also be added to the reaction system simultaneously for the preparation of cosubstituted products, such as boron/phosphorus- and boron/nitrogen-cosubstituted carbon scaffolds. After addition of the reagents, the flask was purged with nitrogen gas, and the mixture was heated to reflux with continuous stirring and held at that temperature for 8 h, whereupon the mixture darkened. The reaction mixture was cooled to room temperature and filtered through a poly(tetrafluoroethylene) (PTFE) membrane with a pore size of 0.45 μm. To completely remove residual salts and organic compounds, the filter cake was washed with 200 mL each of petroleum ether, wet acetone, deionized water, and methanol in sequence. The filter cake was resuspended in ether and filtered, after which the solid was dried in a vacuum oven at 80 °C and a pressure of 30 torr. The product yields were ~0.16 g (67%) for the pristine carbon scaffolds, ~0.18 g (75%) for the boron-substituted scaffolds, ~0.19 g (79%) for the phosphorus-substituted scaffolds, and ~0.22 g (92%) for the nitrogen-substituted scaffolds.

Characterizations. The products were characterized by X-ray photoelectron spectroscopy (XPS), high-resolution transmission electron microscopy (HRTEM), energy-filtered transmission elec-

(7) Leonard, A. D.; Hudson, J. L.; Fan, H.; Booker, R.; Simpson, L. J.; O'Neill, K. J.; Parilla, P. A.; Heben, M. J.; Pasquali, M.; Kittrell, C.; Tour, J. M. *J. Am. Chem. Soc.* **2009**, *131*, 723.
(8) Benard, P.; Chahine, R. *Int. J. Hydrogen Energy* **2001**, *26*, 849.
(9) Zhao, X. B.; Xiao, B.; Fletcher, A. J.; Thomas, K. M. *J. Phys. Chem. B* **2005**, *109*, 8880.
(10) de la Casa-Lillo, M. A.; Lamari-Darkrim, F.; Cazorla-Amoros, D.; Linares-Solano, A. *J. Phys. Chem. B* **2002**, *106*, 10930.
(11) An initial binding energy of 8.5 kJ mol^{-1} on commercially available nanoporous activated carbon fibers has been measured. See: Purewal, J. Hydrogen Adsorption by Alkali Metal Graphite Intercalation Compounds. Ph.D. Thesis, California Institute of Technology, Pasadena, CA, 2010; Appendix A, p 161; http://resolver.caltech.edu/CaltechTHESIS:03042010-183429960 (accessed June 15, 2010).
(12) Burress, J.; Kraus, M.; Beckner, M.; Cepel, R.; Suppes, G.; Wexler, C.; Pfeifer, P. *Nanotechnology* **2009**, *20*, 204026.
(13) Yoon, M.; Yang, S. Y.; Wang, E.; Zhang, Z. Y. *Nano Lett.* **2007**, *7*, 2578.
(14) Yoon, M.; Yang, S. Y.; Zhang, Z. Y. *J. Chem. Phys.* **2009**, *131*, 064707.
(15) Zhang, C. J.; Alavi, A. *J. Chem. Phys.* **2007**, *127*, 214704.
(16) Chung, T. C. M.; Jeong, Y.; Chen, Q.; Kleinhammes, A.; Wu, Y. *J. Am. Chem. Soc.* **2008**, *130*, 6668.
(17) Miwa, R. H.; Martins, T. B.; Fazzio, A. *Nanotechnology* **2008**, *19*, 155708.
(18) Sha, X. W.; Cooper, A. C.; Bailey, W. H.; Cheng, H. S. *J. Phys. Chem. C* **2010**, *114*, 3260.
(19) Yang, S. J.; Cho, J. H.; Oh, G. H.; Nahm, K. S.; Park, C. R. *Carbon* **2009**, *47*, 1585.
(20) Xia, Y. D.; Walker, G. S.; Grant, D. M.; Mokaya, R. *J. Am. Chem. Soc.* **2009**, *131*, 16493.
(21) Mu, T. C.; Huang, J.; Liu, Z. M.; Li, Z. H.; Han, B. X. *J. Mater. Res.* **2006**, *21*, 1658.

tron microscopy (EFTEM) elemental mapping, and Raman spectroscopy. XPS was carried out on a PHI Quantera SXM scanning X-ray microprobe with a base pressure of 5×10^{-9} Torr, an Al cathode X-ray source set at a power of 100 W and a pass energy of 140.00 eV (survey scan) or 26.00 eV (high-resolution scan), a takeoff angle of 45°, and a beam size of 100 μm. Low-resolution survey scans as well as high-resolution scans of carbon, boron, phosphorus, and nitrogen elements were taken. C 1s peaks were normalized and shifted to standard positions. HRTEM and EFTEM mapping were performed using a JEOL 2100F field-emission-gun transmission electron microscope. The EFTEM elemental mappings of carbon and substituted atoms were carried out with the C, B, P, and N K edges at 284, 188, 132, and 401 eV, respectively. Raman spectra of powdered samples were recorded with a Renishaw Raman scope using a 514 nm argon laser.

Hydrogen Uptake Measurements. Hydrogen uptake data at 2 bar and 77 K as well as specific surface areas determined by the Brunauer−Emmett−Teller (BET) nitrogen adsorption method were recorded at the National Renewable Energy Laboratory using a custom instrument[22] that records hydrogen uptake and simultaneously provides heat degassing and records BET surface areas on the same sample without exposure to air. The unique features of this system permitted high-precision measurements for small sample weights, and the temperature and temperature gradients could be accurately controlled across the different zones using copper collars, grafoil gaskets, and a closed-loop thermostatted heat exchanger. The BET surface area data were measured on a Quantachrome Autosorb-1 physisorption system in which the o-ring seals and electrically actuated valves had been replaced by metal seals and pneumatically actuated valves, respectively, in order to increase the thermal stability and accuracy. Before the BET and hydrogen uptake measurements, samples were degassed under vacuum at 200, 400, 500, and 700 °C in order to remove any adsorbed gas, water, or other contaminants, and all of the measurements were repeated after the respective degasses. Hydrogen adsorption isotherms were measured with a custom-built Sieverts apparatus[23] at 77 and 87 K. The Sieverts apparatus was equipped with a high-resolution pressure manometer and high-vacuum molecular drag pump with an oil-free diaphragm backing pump. Hydrogen adsorption isotherms were measured up to 16 bar.

Results and Discussion

As shown in the TEM images (Figure 1), when the reaction was run without the addition of heteroatom precursors, micrometer-scale graphitic carbon sheets were prepared by this bottom-up procedure. Figure 1a shows that the as-obtained graphitic microsheets have a flat flakelike surface on the whole, with ridged wrinkles that may be attributed to lattice defects or uneven stacks of graphene layers. The size distribution of the graphitic microsheets was from several hundred nanometers to ~2 μm. The HRTEM image (Figure 1b; also see section S1 in the Supporting Information) clearly shows the layered structures of the graphitic framework at the edge of the graphitic microsheets. The lighter area of the graphitic microsheets contains 2−5 layers of graphene; 3−5 nm-sized domains of graphene nanoflakes (the dark spots) can also be observed stacked on the surface, indicating that the graphitic microsheets were assembled from smaller graphene domains. While the analytical evidence indicates that graphene nanodomains were produced and assembled under the reaction conditions and it is tempting to invoke the Wurtz reaction on the basis of some similarity to the feedstocks for that reaction, the reaction conditions here are extreme from a solution-phase standpoint, and the mechanism remains unknown but likely involves alkenyl- or arylsodium intermediates.

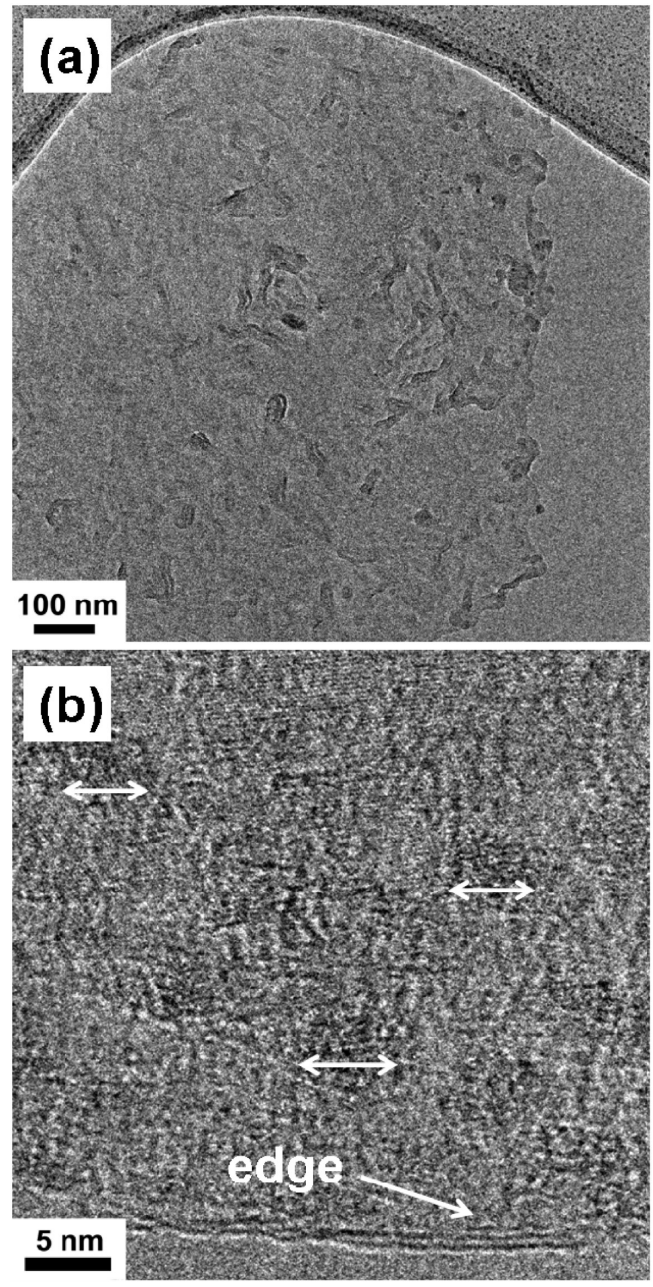

Figure 1. (a) TEM image of pristine carbon scaffold microsheets without heteroatom substitution suspended on a lacy carbon grid. (b) HRTEM image showing the layered graphitic structure at the edge of the carbon scaffold microsheets. Several nanodomains of graphene nanoflakes stacked on the surface of the sheets are indicated by the double-headed arrows.

By addition of the chosen heteroatom precursors in the reaction mixtures, boron-, phosphorus-, and nitrogen-substituted synthetic carbon scaffolds were also prepared. The degree of heteroatom substitution was monitored by XPS, as shown in Figure 2. XPS analyses of the boron-, phosphorus-, and nitrogen-substituted products (also see the survey scans in section S2 in the Supporting Information) indicated the presence of added elements in the substituted carbon scaffolds. High-resolution XPS of samples showed the atomic percentages of substituted

(22) Simpson, L. J.; Parilla, P. A.; Blackburn, J. L.; Gennett, T. G.; Gilbert, K. E. H.; Engtrakul, C.; Dillon, A. C.; Heben, J. M. In *Global Progress Toward Clean Energy*, Proceedings of the 17th NHA Annual Hydrogen Conference, Long Beach, CA, March 12−16, 2006 (DVD-ROM); National Hydrogen Association: Washington, DC, 2006; p 14.

(23) Purewal, J. J.; Kabbour, H.; Vajo, J. J.; Ahn, C. C.; Fultz, B. *Nanotechnology* **2009**, *20*, 204012.

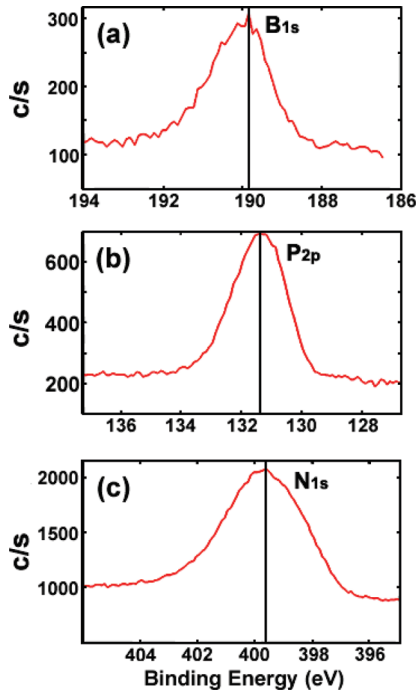

Figure 2. High-resolution XPS scans of the substituted elements in the carbon scaffolds: (a) boron; (b) phosphorus; (c) nitrogen.

elements were as high as 7.3% for boron, 8.1% for phosphorus, and 28.1% for nitrogen, indicating that the substitution efficiency of this approach is high. No obvious chlorine peaks were detected; the fraction of Cl in the samples was normally less than 0.4%, indicating that chlorine had been sufficiently removed from the original precursors and excluded from the carbon scaffolds by reaction with sodium and eventual coupling or protonolysis upon workup. Oxygen peaks, normally corresponding to less than 1.0% O, were observed, possibly as a result of surface adsorption or slight surface oxidation after exposure to atmosphere. The position of the B 1s peaks in the XPS spectrum at ~189.9 eV is indicative of boron substitution in the sp^2 carbon framework, as it is similar to the peak position of boron in BC_3 films[24] and BC_x nanotubes.[25] The P 2p signal at 131.4 eV was shifted to lower binding energy relative to the P−O peak normally found near 134 eV because of phosphorus atoms fixed in the carbon scaffolds. The nitrogen-substituted carbon scaffolds had only one peak at ~399.6 eV, which is different from the N 1s peaks of CN_x materials prepared by other methods,[19,20] indicating that only a single type of nitrogen atom is present. It is likely the cyanuric structures were preserved in the carbon scaffolds. Cosubstituted carbon scaffolds with two substitution elements were also prepared. XPS analysis showed that the atomic percentages in the boron/phosphorus-cosubstituted sample were 4.5% boron and 4.2% phosphorus, while in the boron/nitrogen-cosubstituted sample, the atomic percentages were 3.2% boron and 10.3% nitrogen.

The heteroatom-substituted samples of synthetic carbon scaffolds were also characterized by TEM, as shown in Figure 3. In comparison with the pristine carbon scaffolds, the degree of crystallinity of the heteroatom-substituted carbon scaffolds was decreased, as expected. On the other hand, the micropores and binding energies of the carbon scaffolds can be improved by heteroatom substitutions, which should increase hydrogen storage. In the nitrogen-substituted samples, in addition to the sheet structures, nanotube- and nanowhisker-like structures were also observed (Figure 3d), an indication that the high substitution ratio of nitrogen atoms in the carbon framework impacted the morphology of the products.

To assess the homogeneity of the heteroatoms in the substituted carbon scaffolds, elemental mapping with EFTEM was performed. As shown in Figure 3 and in section S3 in the Supporting Information, the substituted heteroatoms (red dots) were uniformly spread throughout the carbon scaffolds (carbon atoms are represented by green dots). The concentration of heteroatoms changed with the thickness of the flakes, indicating not only that substituted atoms were located on the surface of the carbon scaffolds but also that the substitution occurred in the interior basal planes of the carbon scaffolds.

Raman spectra of the pristine and heteroatom-substituted carbon scaffolds are displayed in Figure 4. The D/G band intensity ratio reveals the in-plane crystallite dimension and the degree of in-plane defects and edge defects in the carbon materials. The D/G peak height ratio of the pristine carbon scaffolds was ~0.4. Following the addition of heteroatoms, the D band became higher and broader. The value of the D/G peak ratio increased to ~0.7 as the boron or phosphorus substitution was introduced into the carbon network, indicating that the degree of disorder of the material structure increased, as expected. The D/G peak ratio of the nitrogen-substituted samples increased to ~0.9, indicating that the degree of long-range-ordered crystallinity was decreased by the very high proportion of nitrogen substitution.

BET surface area measurements of the pristine and heteroatom-substituted carbon scaffolds were obtained after degassing at different temperatures, and hydrogen uptake data at 77 K and 2 bar were collected simultaneously. After a series of tests, degassing at 500 °C was found to be optimal for maximizing the specific surface area. The surface area of the pristine carbon scaffolds was found to be as high as 700 $m^2\ g^{-1}$. The boron- and phosphorus-substituted samples had surface areas of ~900 and 700 $m^2\ g^{-1}$, respectively, while the nitrogen-substituted samples had a surface area of 200−300 $m^2\ g^{-1}$, which indicates that it has a more compact structure with less porosity because of the very high concentration of substituted nitrogen heteroatoms. Figure S4 in the Supporting Information shows the pore size distributions of pristine and heteroatom-substituted carbon scaffolds; the heteroatom-substituted carbon scaffolds exhibited narrow peaks in the 2.3−2.8 nm pore diameter range that are larger than the peaks due to pristine carbon scaffolds in the same range.

Plotting the hydrogen uptake versus the surface area provides the hydrogen storage capacity per unit surface area, as shown in Figure 5. The hydrogen uptake capacity of pristine carbon scaffolds was 1.8 wt % per 1000 $m^2\ g^{-1}$. The hydrogen uptake of boron- and phosphorus-substituted samples showed a linear relationship with the specific surface area and had values of 2.2 and 2.4 wt % per 1000 $m^2\ g^{-1}$, respectively, at 77 K and 2 bar, demonstrating an enhancement of the hydrogen uptake capacity relative to the pristine carbon scaffolds. These data indicate that with the aid of substituted heteroatoms in the carbon scaffolds, the binding of hydrogen molecules can be significantly improved. Nitrogen-substituted products with relatively low surface areas appeared to enhance the hydrogen uptake capacity per unit surface area. Meanwhile, the hydrogen uptake capacities of the boron/phosphorus- and boron/nitrogen-cosubstituted

(24) Fecko, D. L.; Jones, L. E.; Thrower, P. A. *Carbon* **1993**, *31*, 637.
(25) Satishkumar, B. C.; Govindaraj, A.; Harikumar, K. R.; Zhang, J. P.; Cheetham, A. K.; Rao, C. N. R. *Chem. Phys. Lett.* **1999**, *300*, 473.

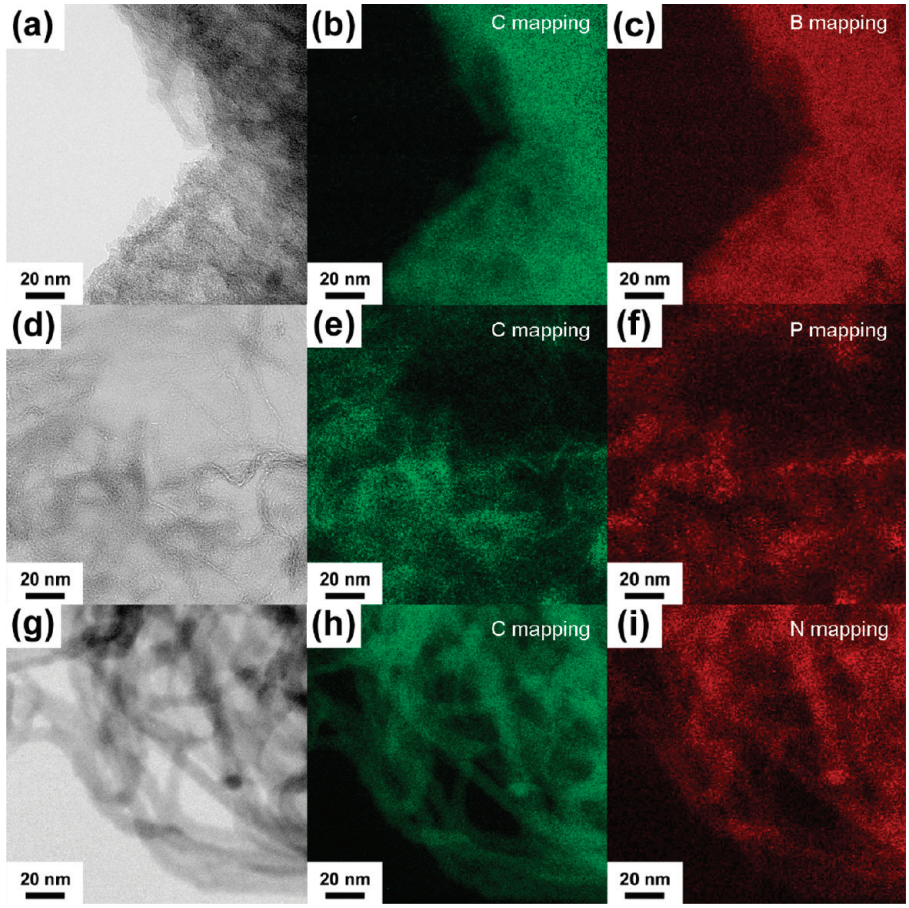

Figure 3. TEM images (left) and EFTEM elemental mappings of carbon (middle) and substituted elements (right) of heteroatom-substituted carbon scaffolds: (a−c) boron; (d−f) phosphorus; (g−i) nitrogen. The carbon atoms are represented by green dots and the substituted heteroatoms by red dots.

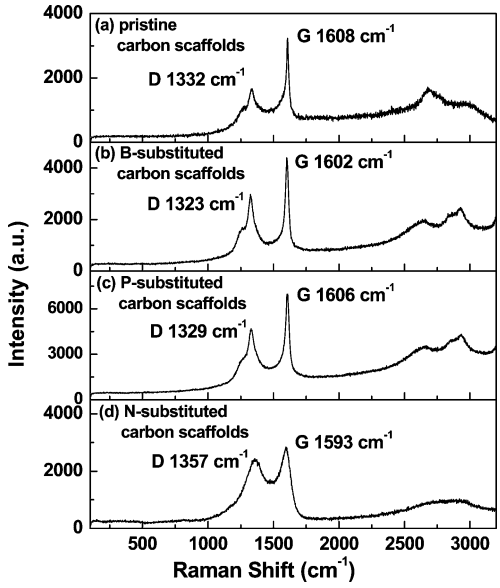

Figure 4. Raman spectra (514 nm) of (a) pristine carbon scaffolds and (b) boron-, (c) phosphorus-, and (d) nitrogen-substituted synthetic carbon scaffolds.

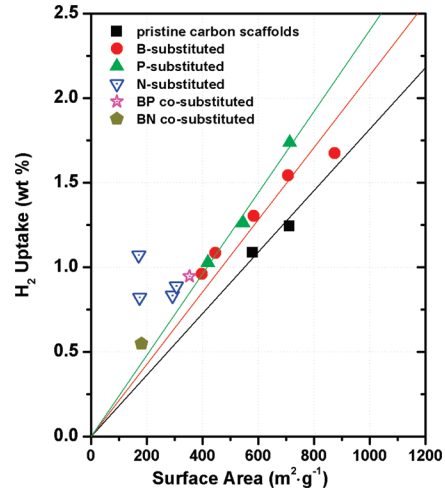

Figure 5. Hydrogen uptake at 77 K and 2 bar vs BET specific surface area measured using nitrogen at 77 K. The data for pristine and substituted carbon scaffolds are indicated by the different colored symbols, as shown in the legend. The solid lines with the matching colors are linear fits and extrapolations obtained from the sample data.

products were also measured; the values for the cosubstituted samples were slightly higher than those of the boron- or phosphorus-substituted samples. Also, placing the sample powders into solvent mixtures with different densities and determining their neutral buoyancies showed that the density of the substituted carbon scaffolds was ~1.5 g·cm^{-3}, which is higher than that of typical carbon adsorbents[10] and thus gives a better volumetric capacity.

The hydrogen binding energies of the three substituted carbon scaffold samples were estimated by measuring hydrogen adsorption isotherms at 77 and 87 K and applying the isosteric method, as shown in Figure 6. The isotherm data were fitted to

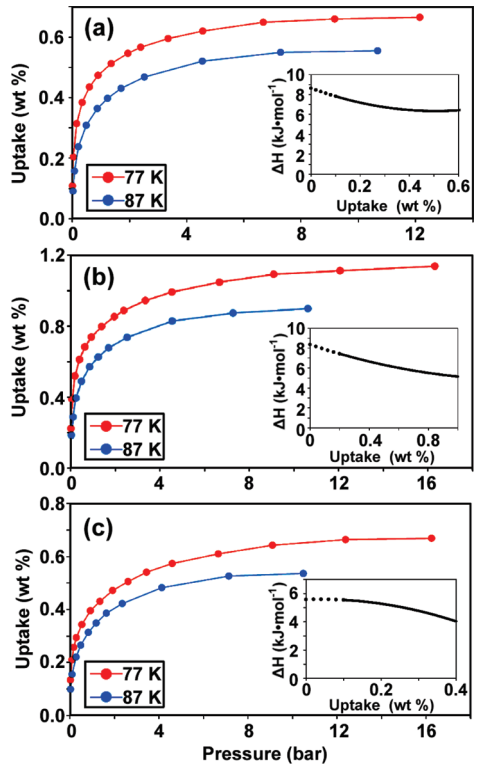

Figure 6. Hydrogen adsorption isotherms of (a) boron-, (b) phosphorus-, and (c) nitrogen-substituted carbon scaffolds at 77 and 87 K. The corresponding insets show the relationships between the hydrogen uptake capacity and the heat of adsorption; the binding energies of hydrogen were deduced by extrapolation of the adsorption enthalpy to zero coverage.

a particular virial-type thermal equation of gas−solid adsorption,[26] and the adsorption amounts at different pressures were then converted to the heat of adsorption, ΔH, using the Clausius−Clapeyron equation (eq 1):

$$\Delta H = R\frac{\mathrm{d}\ln P}{\mathrm{d}(1/T)} \qquad (1)$$

where T and P are the system's temperature and pressure, respectively, and R is the universal gas constant.[27,28] The calculation process is described in detail elsewhere.[29] From the plots of hydrogen uptake versus pressure (Figure 6), the isosteric heats of adsorption at zero coverage for the boron-, phosphorus- and nitrogen-substituted carbon scaffolds were estimated by extrapolation. Thus, we obtained the following hydrogen binding energies for the heteroatoms: boron, 8.6 kJ mol^{-1}; phosphorus, 8.3 kJ mol^{-1}; nitrogen, 5.6 kJ mol^{-1}. The binding energies for the boron- and phosphorus-substituted samples are considerably higher than those for typical unsubstituted carbon materials (4−6 kJ mol^{-1}).[9,30] The nitrogen-substituted samples showed a small enhancement of the binding energy; however, the very high concentration of the nitrogen heteroatoms (28%, which is 3−4 times higher than the concentration of boron or phosphorus heteroatoms) might provide additional binding sites for hydrogen molecules. Second, the stable cyanuric structures in the carbon scaffolds derived from the nitrogen-containing precursors might produce nanocavities that could be beneficial for trapping hydrogen molecules.[19] The higher hydrogen capacity per unit specific surface area for the nitrogen-substituted carbon scaffolds could be attributable to the pore size distribution. As shown in Figure S4d in the Supporting Information, in contrast to the pristine and boron- or phosphorus-substituted carbon scaffolds, the pore size distribution graph for the nitrogen-substituted carbon scaffolds has a smaller shoulder peak extending to smaller pore sizes. This is an indication that the nitrogen-substituted carbon scaffold has fewer pores with diameters less than 2.0 nm. Moreover, nitrogen atoms are good binding sites for a variety of metal atoms, which in turn might considerably increase the binding energy of the hydrogen, so the nitrogen substitution has the possibility of being beneficial in a different motif.[31,32]

Summary

We have developed a facile process for the bottom-up preparation of synthetic carbon scaffolds with good surface areas and successfully achieved the synthesis of carbon scaffolds containing boron, phosphorus, and nitrogen heteroatoms in high atomic percentages. The heteroatom-substituted carbon scaffolds have enhanced hydrogen physisorption capacities and hydrogen binding energies relative to pristine carbon scaffolds and common carbonaceous materials.

Acknowledgment. Financial support was provided by the U.S. Department of Energy's Office of Energy Efficiency and Renewable Energy within the Hydrogen Sorption Center of Excellence at the National Renewable Energy Laboratory (DEFC-36-05GO15073).

Supporting Information Available: Additional HRTEM images of pristine carbon scaffolds, XPS spectra of pristine and heteroatom-substituted carbon scaffolds, additional EFTEM elemental mapping plots of heteroatom-substituted carbon scaffolds, and pore size distributions of pristine and heteroatom-substituted carbon scaffolds. This material is available free of charge via the Internet at http://pubs.acs.org.

JA105428D

(26) Czepirski, L.; Jagiello, J. *Chem. Eng. Sci.* **1989**, *44*, 797.
(27) Pan, H. H.; Ritter, J. A.; Balbuena, P. B. *Langmuir* **1998**, *14*, 6323.
(28) Hilding, J. M.; Grulke, E. A. *J. Phys. Chem. B* **2004**, *108*, 13688.
(29) Purewal, J. Hydrogen Adsorption by Alkali Metal Graphite Intercalation Compounds. Ph.D. Thesis, California Institute of Technology, Pasadena, CA, 2010; Chapter 3, p 47; http://resolver.caltech.edu/CaltechTHESIS:03042010-183429960 (accessed June 15, 2010).
(30) Benard, P.; Chahine, R. *Langmuir* **2001**, *17*, 1950.
(31) Kim, G.; Jhi, S. H.; Park, N. *Appl. Phys. Lett.* **2008**, *92*, 013106.
(32) Zhang, Y.; Sun, H.; Chen, C. F. *Phys. Lett. A* **2009**, *373*, 2778.